공학석사학위논문

Integrated Design of Tailless FWMAV with free play: Approach via Geometry and Numerical Analysis

유격을 고려한 무미익 초소형 날갯짓 비행체 통합 설계: 기하분석 및 수치 해석을 통한 접근

2021년 2월

서울대학교 대학원

우주시스템전공

최 재 원

Integrated Design of Tailless FWMAV with free play: Approach via Geometry and Numerical Analysis

유격을 고려한 무미익 초소형 날갯짓 비행체 통합 설계: 기하분석 및 수치 해석을 통한 접근

지도교수 신 상 준

이 논문을 공학석사 학위논문으로 제출함

2021 년 2 월

서울대학교 대학원

우주시스템전공

최 재 원

최재원의 공학석사 학위논문을 인준함

2021 년 2 월

위 원 장 윤 군 진 (인)

부위원장 신 상 준 (인)

위 원 조 해 성 (인)

Abstract

Integrated Design of Tailless FWMAV with free play: Approach via Geometry and Numerical Analysis

JaeWon Choi

Interdisciplinary Program in Space System

The Graduate School

Seoul National University

Unlike birds, an insect type tailless flapping wing does not possess tail wings. Therefore, insect type flapping wing may be fabricated in small size and of decreased weight. Because of the taillessness, however, stable flight of an insect type flapping wing depends only on main wings. Thus, a number of researches were conducted regarding its control mechanisms. In this thesis, the trailing edge control, one of the methods developed to produce control moments, is adopted. Such method requires additional shafts that connect the root of the main wing and control mechanism, and the shafts are rotated to deform the wing shape. In this manner, asymmetric aerodynamic forces are produced. The control mechanism uses micro actuators for compact design. However, small size of the micro actuator gearbox causes relatively large backlash and the resulting free play of the main wings that generates undesirable aerodynamic forces.

Under such circumstance, design improvement of the control mechanism is conducted to minimize the effects of the free play. First, geometry analysis is

performed to investigate the factors that cause the free play. Control mechanism design for the minimized free play is obtained. Then, three-dimensional computer aided design (CAD) of modified configuration is drawn, and kinematic simulations are conducted by RecurDyn to determine the prevention of interference. Finally, the feasibility of modified design is examined by the numerical simulation. The main wings are modeled by the displacement-based geometrically exact beam model combined with cross-sectional analysis. To mimic the free play appropriately, the spring elements are attached to the joints. At the same time, two-dimensional unsteady aerodynamic model is used for aerodynamic forces. Consequently, the reasonable control moments are gathered in terms of the maneuverability.

Keywords: insect-type flapping wing, free play, geometry analysis, numerical simulation

Student Number : 2019-22226

Contents

Page

List of Tables

Page

List of Figures

Page

List of Symbols

Symbols	Meaning
r_1	rolling linkage length, mm
r_2	pitching-yawing linkage length, mm
r_3	main wing shaft length, mm
l_1	rolling linkage margin length, mm
l_2	pitching linkage margin length, mm
θ_1	rolling actuator rotation angle, degrees
θ_2	pitching-yawing actuator rotation angle, degrees
θ_3	main wing shaft rotation angle, degrees
θ_4	rolling linkage rotation angle, degrees
h_1	rolling actuator distance from top of the device, mm
h_2	pitching-yawing actuator distance from top of the device, mm
h_3	multi-DOF link length, mm

Preface

This thesis is based on the following publications and manuscripts.

Conference 1

Choi, JW., Gong, DH., Yoon, NK., and Shin, SJ., "Design and Free Play Analysis for a Control Mechnism of an Insect-Type FWMAV," 2021 AIAA Scitech Forum, 2021. (To be presented)

Chpater 1

Introduction

1.1 Background

Recently, a large number of researches on micro aerial vehicles (MAV) have been conducted to take the advantages of the compact dimensions and the decreased weight. MAV can be divided into the following three types: fixed-, rotary-, and flapping wing. Among those, the types of flapping wing MAV (FWMAV) are further divided into bird [1-2] and insect-type [3-5]. Those types of aircraft mimic flyers in the nature for the high aerodynamic efficiency and agile maneuverability. Figure 1.1 shows configuration of the bird and insect-type bio-inspired flapping wing. The major difference in the two types of aircraft is the existence of the tail wings. The bird-type flapping wing use the tail wings for altitude stabilization or control of the heading angle. On the contrary, an insect-type tailless flapping wing use only main wings for stable flight. Consequently, insect-type flapping wing can be fabricated in a compact size compared to the bird type ones. Being smaller in size and not having a tail, it may become quite lighter.

Given the characteristics of small size and hover capability, insect-type flapping wing can freely maneuver and take off in confined spaces. Due to those advantages as mentioned above, insect-type flapping wing can be employed for various missions in fields of military and civilian, such as reconnaissance, video surveillance and rescue missions. However, the features of small size demand the complex design mechanism. Also oscillatory motion occurs by the smaller weight with high flapping frequency, and consequently results in difficulties of the controllability. Additionally, peculiarity of the tailless flapping wing requires main wings to produce not only the thrust and drag, but also the control moments.

Therefore, design and control of the insect-type tailless flapping wing will be a challenging task.

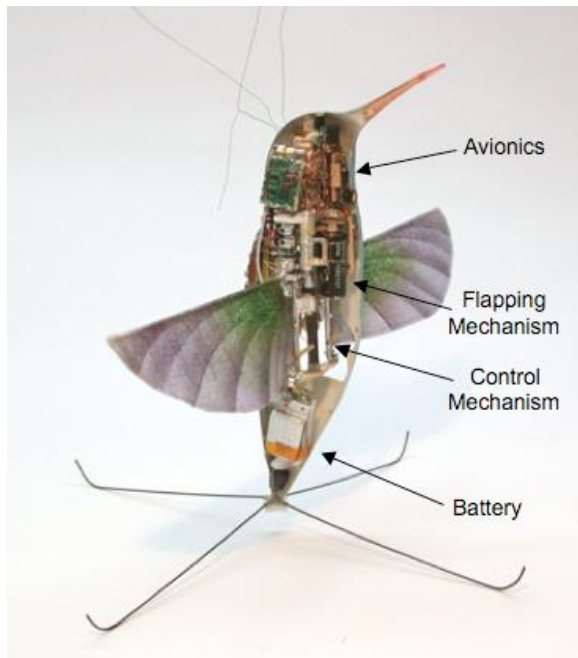

(a) Insect-type flapping wing [5]

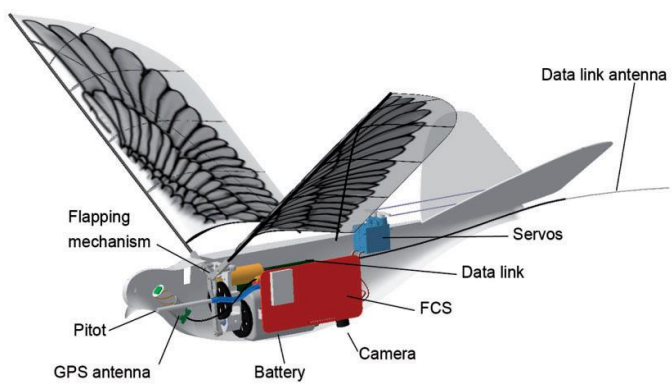

(b) Bird-type flapping wing [2]

Figure 1.1 Types of bio-inspired flapping wing

1.2 Previous Researches

In this section, previous researches regarding to control mechanism design and flight simulation of FWMAV will be presented. As aforementioned descriptions, usual tailless insect-type flapping wing is designed to be able to maneuver and maintain the stable attitude using only main wings as shown in Figure 1.2. Because of these reasons, active and vibrant researches regarding control mechanisms of FWMAV have been conducted.

1.2.1 Review of the Control Mechanism Design Regarding the Insect-Type Flapping Wing

Various methods were adopted to control the postures of a flapping wing, such as varying the shape of the wings, stroke plane, or flapping frequencies of each wing.

Nano Hummingbird developed by AeroVironment [5] was the tailless FWMAV of which mass and wingspan were 19g and 16.5cm, respectively. For maneuverability, the control mechanism was designed to generate the wing twist and rotation modulation. Asymmetric angle of attack caused asymmetric forces and the control moment induced were measured.

Phan et al. [6] designed an insect-type FWMAV, named KUBeetle. The tailing edge control method was employed to generate the control moments: roll, pitch, and yaw. Also, they fabricated the prototype of FWMAV and measured the control moments with a 6-axis load cell to verify the capability of the control mechanism to generate a reasonable control moment.

In addition, Gong [7] designed a modularized control mechanism which was independent of flapping mechanisms, and could be combined with several specific flapping mechanisms. This type of control mechanism required two DC motors to produce the pitching and rolling moments. Hence, the mechanism could be fabricated with small weight. However, the

mechanism was unable to generate the yawing moments. And use of DC motors to operate a mechanism hindered to adjust control forces continuously.

The previous studies regarding the design of control mechanisms achieved maneuverability without control surface. Furthermore, various ideas paved the way for improved control mechanism of the tailless flapping wing.

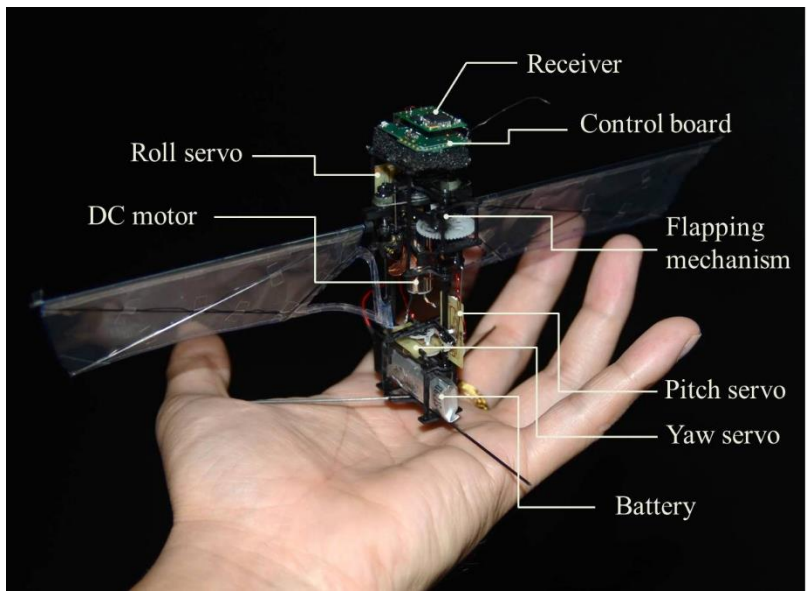

(a) KUBeetle [6]

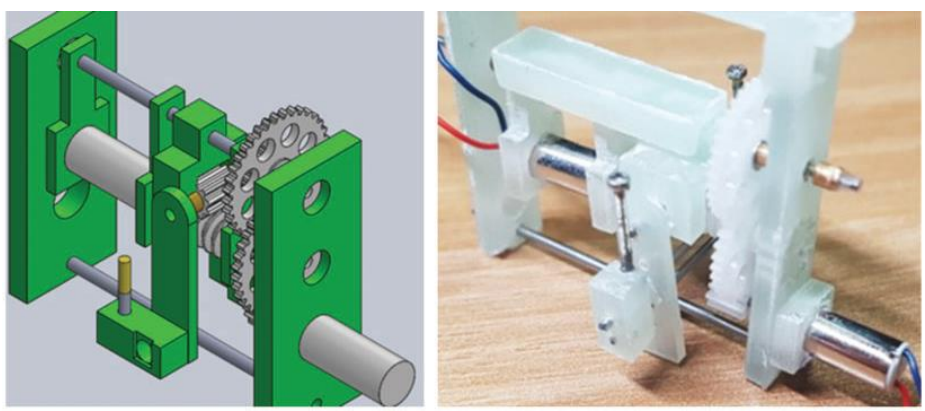

(b) Drawing and the prototype of the control mechanism [7]

Figure 1.2 Configurations of the bio-inspired flapping wing

1.2.2 Review of Numerical Simulation Studies Regarding the Insect-type Flapping Wing

The numerical simulations of the insect-type FWMAV have been widely conducted due to the feature of inherent instability. In addition, numerical simulations are used in the flight controller design.

Hassan and Taha [8] studied numerical simulation for hover of the insect-type flapping wing. They studied aerodynamic-dynamic interactions to identify the relationship between fast, periodic, aerodynamic wing forces and relatively slow body motion. Also, they revealed a vibrational stabilization mechanism which contributed to the body pitch stabilization. Flappy Hummingbird, an open-source dynamic simulation, was developed by Fei et al. [9]. They used different flapping frequencies for each wing to produce an asymmetric force. The blade element theory and quasi-steady aerodynamic model were adopted to simulate take-off and altitude tracking. In addition, they constructed a simple PID flight controller based on the simulation results.

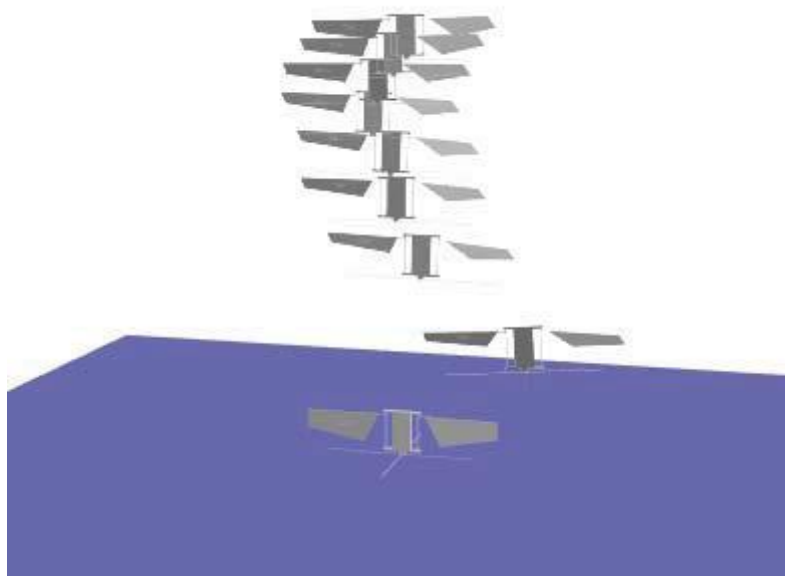

Figure 1.3 Take-off simulation [9]

1.3 Research Objectives and Thesis Outline

This thesis conducts design and analysis of an improved control mechanism which produces 3-axis flight control moments. In many mechanisms, free play exists in actuators due to backlash of the gearbox. Such free play may cause instability and degradation of controllability by undesirable aerodynamic forces. The free play is to be minimized by the geometry analysis. Also, numerical simulation is to be performed to verify the present control mechanism. The remainder of this thesis is organized as follows:

Chapter 2 describes the free play effect on the insect type flapping wing, and introduces geometry analysis conducted for the design control mechanism to minimize the free play effect.

Chapter 3 provides numerical simulation of FWMAV, and presents multi-body dynamic model validated by the numerical simulation.

Chapter 4 presents a conclusion of the thesis and future works to be implemented.

Chapter 2

Control Mechanism Design with a Free play

2.1 Overview of Control Mechanism Design with a Free play

This section provides an overview of the design of a free play control mechanism. The micro actuators are used for insect-type FWMAV because of their small weight and compact size. In this regard, plastic gears are installed in the gearbox, which account for a significant portion of the total weight. Therefore, compared to a large actuator, there is inevitable large free play due to the backlash of the gear. Nevertheless, few studies have focused on the free play of FWMAV [10-11].

In the present thesis, the free play of the actuators is considered for a valid design of the control mechanism. In order to minimize the free play, appropriate linkage length and actuator location are determined. The initial mechanism design by the authors is shown in Figure 2.1. In such configuration, the actuators are arranged on top of the frame, and connected directly to the gears of the main wing shafts. Thus, the torque of the actuators is transmitted to the gear without loss. However, the free play effect can be amplified by long moment arm of the main wing shafts. In Figure 2.1, the white curve in the figure represents the free play of the actuator, and the red line represents the free play amplified by the linkage. Therefore, the actuators should be located at the bottom of the frame and an additional connector is required to connect the main wing shafts.

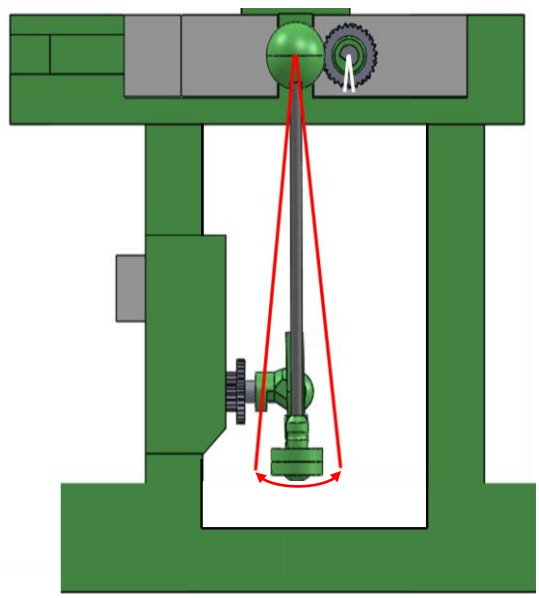

Figure 2.1 Configuration of the control mechanisms

2.2 Control Mechanism: Trailing Edge Control

The schematic of the present wing is shown in Figure 2.2. The wings are constructed of the carbon rods, sheets and mylar sheets. Made of the carbon rods, the leading edge vein are located on the leading edge to intertwine wings to the fuselage. Furthermore, veins of carbon sheets, which are arbitrary arranged on the wing surface, primarily take for the structural stiffness of the wing. Mylar sheets are stiffened by the leading edge veins and additional shafts. The shape of the main wings can be deformed by the aerodynamic pressure due to the mylar flexibility.

In order to generate the control moments, the method of trailing edge control (TEC) is adopted [5,12]. This method will twist the trailing edges of wings to change the camber as shown in Figure 2.3. Consequently, instantaneous differences in angles of attack can be obtained in each wing. Therefore, the control moments will be introduced due to asymmetrically distributed air load. The additional shaft which is aforementioned can be rotate around x- and y-axis. Reasonable control moments, rolling, and pitching can be produced by appropriate rotating motions of the additional shafts which are located at wing roots. The trailing edge control mechanism in accordance with rolling, and pitching is shown in Figure 2.4.

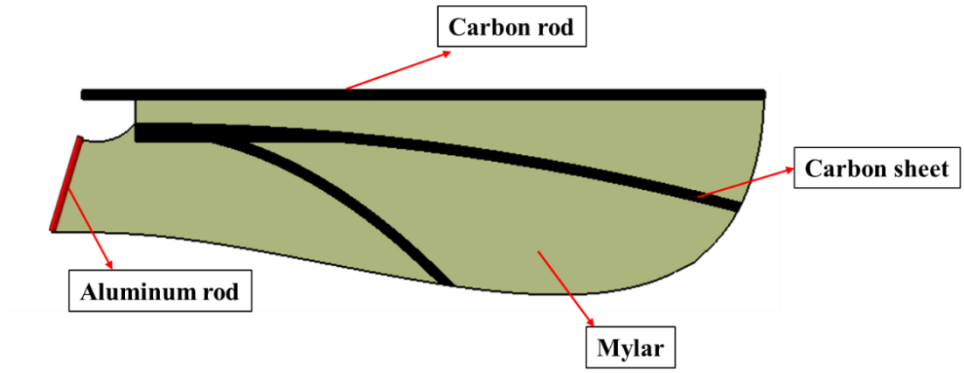

Figure 2.2 Configuration of the main wing [13]

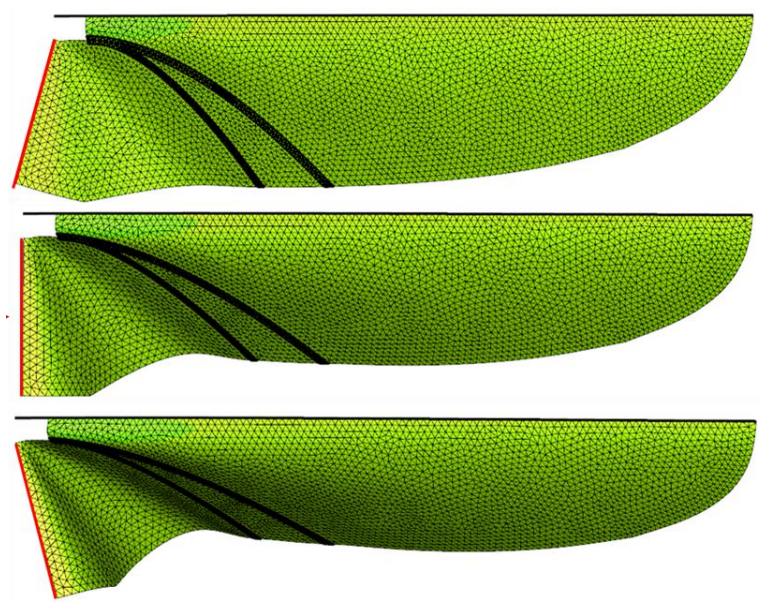

Figure 2.3 Additional shaft modulation

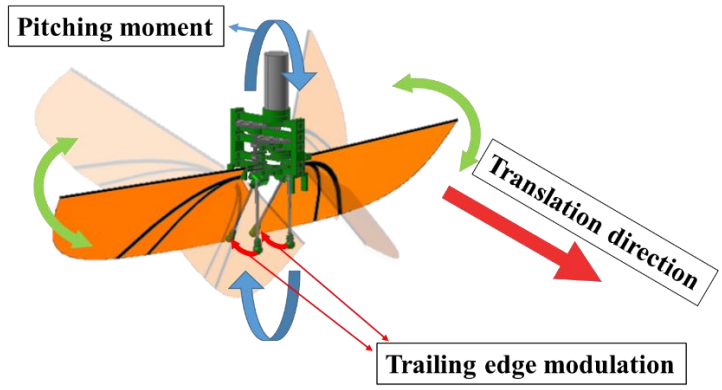

(a) Pitching moment generation via wing twist modulation

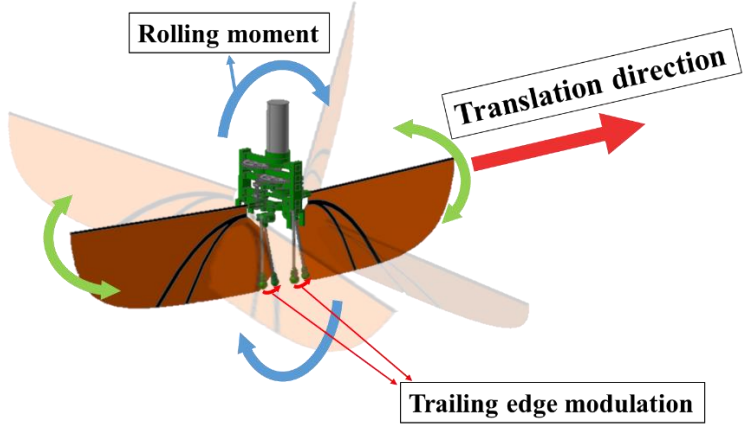

(b) Rolling moment generation via wing twist modulation

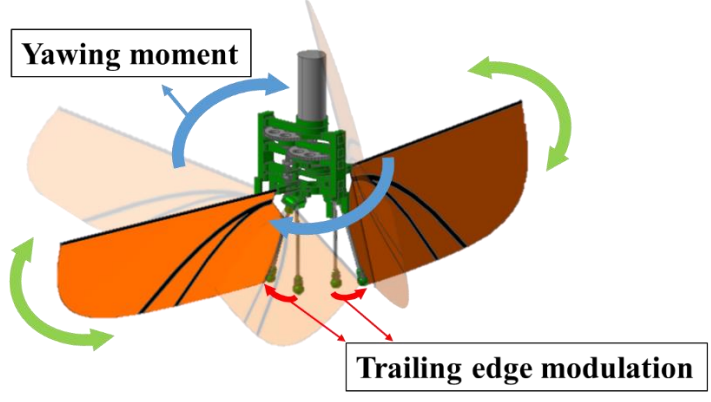

(c) Rolling moment generation via wing twist modulation

Figure 2.4 Trailing edge control

2.3 Components of the Control Mechanism

A number of components are used as shown in Figure 2.5 to generate the desired control motions. Also, to twist the trailing edge, the root of the main wing is connected to the main wing shaft. The wing root consists of a mylar that is wound around the main shaft for free rotation during the flapping motions. Two pitching-yawing linkages and one rolling linkage are used for the control mechanism to generate the control motions. Those linkages are driven by three actuators, and shift a multi-degree-of-freedom link located at the middle of the frame. Also, outer shell of the actuators and unnecessary components are removed to save the weight of the control mechanism. The multi-degree-of-freedom link, which is shown in Figure 2.6, connects the three actuators and the main wing root shafts. Multi-degree-of-freedom link consists of two 4-mm spherical slide bearings, one cylindrical sliding joint, one sliding joint, and two ball joints. The purpose of such link is to disconnect the force being transmitted from one actuator to the other.

In order to generate the pitching moment, two actuators at the bottom will rotate the linkage in the same direction. If they operate in the opposite directions, yawing moment will be generated. Rolling moment is generated by an actuator mounted on the middle of the frame, which drives both linkages in the same direction by connected multi-degree-of-freedom link.

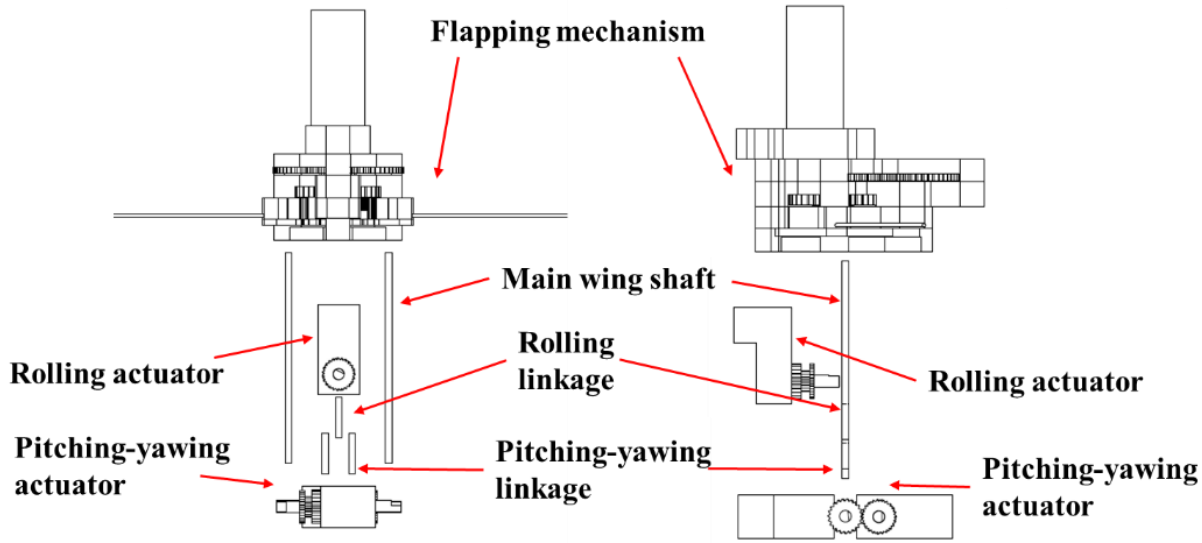

Figure 2.5 Components of the present control mechanism

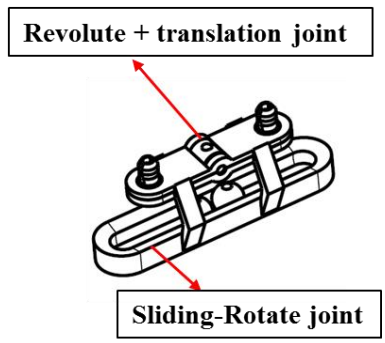

(a) Isometric view

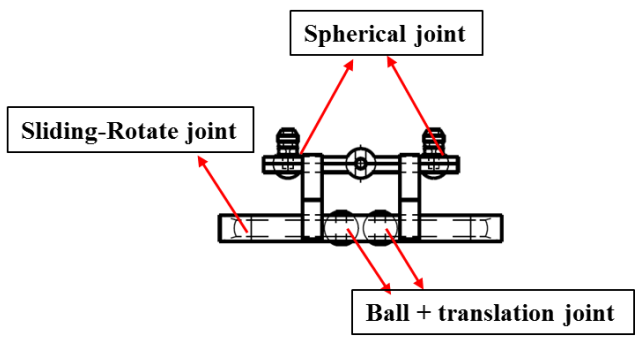

(b) Front view

Fig. 2.6 Schematics of the multi-degree-of-freedom link

2.4 Control Mechanism Design with Minimize free play effect

In order to minimize the free play appropriate linkage length and actuator location should be determined beforehand. The free play of the actuator is approximately $\pm 3°$ in average, which is produced by backlash of the gearboxes. The free play intensified by linkage may cause excessive vibration at the wing root, resulting in degraded aerodynamic efficiency. Also, this phenomenon is affected by the linkage length, which acts as a moment arm. Therefore, by reducing the length of the linkage, free play at the shaft can be decreased. However, in opposite, the operation radius will be dwindled. Hence, geometry analysis will be required for stable control mechanism design.

To prevent the linkage being separated from the spherical slide bearing and cylindrical revolute joint, the turning radius of the actuator is limited to $\pm 60°$. Based on Phan et al. [6], the wing twist angle θ_3 is set to be 10°. From the restrictions of the present flapping mechanism and size, the distance between main shafts is 15mm. The length of the main shafts r_3 is set to 25mm for assembly with several wings which are of different root length, 20mm to 25mm. The geometry of the present control mechanism is shown in Figure 2.7. The rolling linkage length is determined by Equation (1). Also, since the components are clustered inside the TEC module, interference among the components should be carefully inspected. Especially, during the yawing motion, the rolling linkage may interfere with the spherical slide bearings. In order to prevent such phenomenon, the relevant length, l_1 and l_2, should be carefully determined.

l_1 and l_2 can be estimated by Equations (2) and (3).

$$r_1 = \frac{r_3 \sin\theta_3}{\sin\theta_1} \tag{1}$$

$$l_1 = r_1(1 - \cos\theta_1) \tag{2}$$

$$l_2 = r_2(1 - \cos\theta_2) \tag{3}$$

Using Equation (1), the rolling actuator location h_1 and rolling linkage rotation angle θ_4 can be found. Also, the multi-degree-of-freedom link length h_3 is determined by Equations (2) and (3)

$$h_1 = r_3 \cos\theta_3 - \sqrt{r_1^2 - r_3^2 \sin^2\theta_3} \tag{4}$$

$$\theta_4 = \sin^{-1}\left(\frac{r_3 \sin\theta_3}{r_1}\right) \tag{5}$$

$$h_3 = l_1 + l_2 \tag{6}$$

Finally, using Equations (1)-(6), the yawing-pitching linkage length r_2 and the pitching-yawing actuator location h_2 can be obtained.

$$r_2 = \sin\theta_4 \frac{r_1(2 - \cos\theta_1)}{\sin\theta_2 + \sin\theta_4(\cos\theta_2 - 1)} \tag{7}$$

$$h_2 = h_1 + (r_1 + h_3)\cos\theta_4 + r_2 \cos\theta_2 \tag{8}$$

To minimize intensified linkage length, a simple average of the linkage lengths is selected as the objective function. Also, the operation radii θ_1 and θ_2 are used for the decision variables. In order to obtain a similar intensified free play in each actuator, Equation (9) is selected for constraints. Furthermore, Equations (10) and (11) are other inequality constraints to consider actuator turning radius.

$$r_1 - r_2 < 0.1mm \tag{9}$$

$$\theta_1 < 60° \tag{10}$$

$$\theta_2 < 60° \tag{11}$$

Figure 2.8 shows the contour plot for the objective values as a function of rolling actuator rotation angle and pitching-yawing actuator rotation angle. The red line represents the

objective value which satisfies the first constraint aforementioned. In addition, the magenta-colored area at the top of Figure 2.8 represents the constraint of the turning radius of the pitching-yawing actuator, while the black area on the right-hand represents another constraint of the turning radius of the rolling actuator. Therefore, the point of green cross can be obtained that satisfies all constraints while minimizing average linkage length. Furthermore, the location of the actuators that satisfies the required operation radii while minimizing the free play will be obtained.

From Equations (1) -(8) and constraints mentioned above, the lengths of the linkages and frame are obtained as summarized in Table 2.1 Three-dimensional drawings are suggested from the parameters found in the table. The black line at the actuator shown in Figure 2.9 represents the free play of the actuator, while the red line represents the free play amplified by the linkage. The intensified free play of the modified configuration is 0.9mm. Consequently, the free play is significantly reduced compared to 2.6mm in the initial design.

Also, a kinematic simulation is performed which considers the practical volume of the components such as joints, actuators and linkages. For the analysis, commercially available software, RecurDyn is adopted. First, a three-dimensional computer aided design (CAD) drawing is performed based on the parameters listed in Table 2.1. Then each rolling, pitching, and yawing, is simulated by RecurDyn as shown in Figure 2.10. As a result, no interference is found in the three types of control motions.

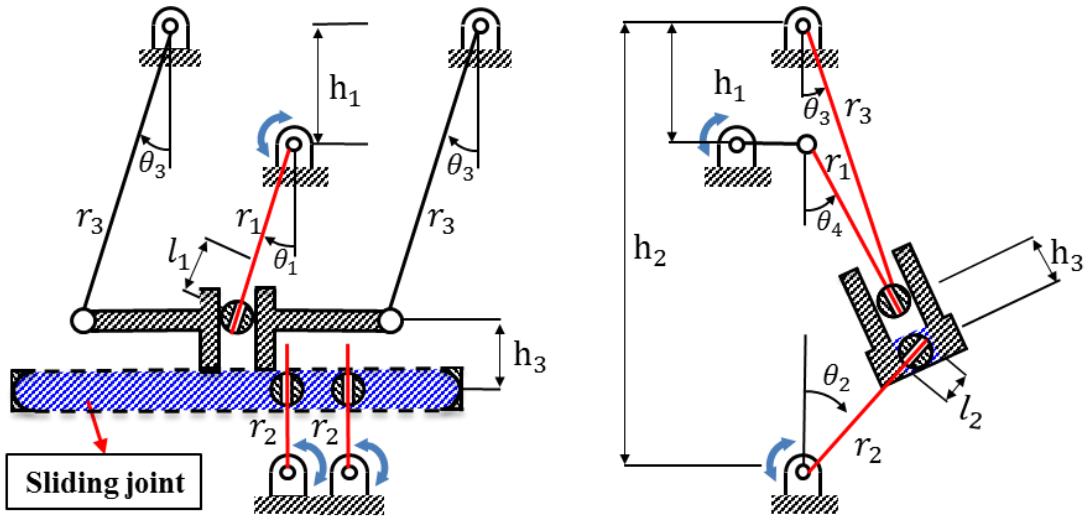

Figure 2.7 Geometry for the present control moment generation

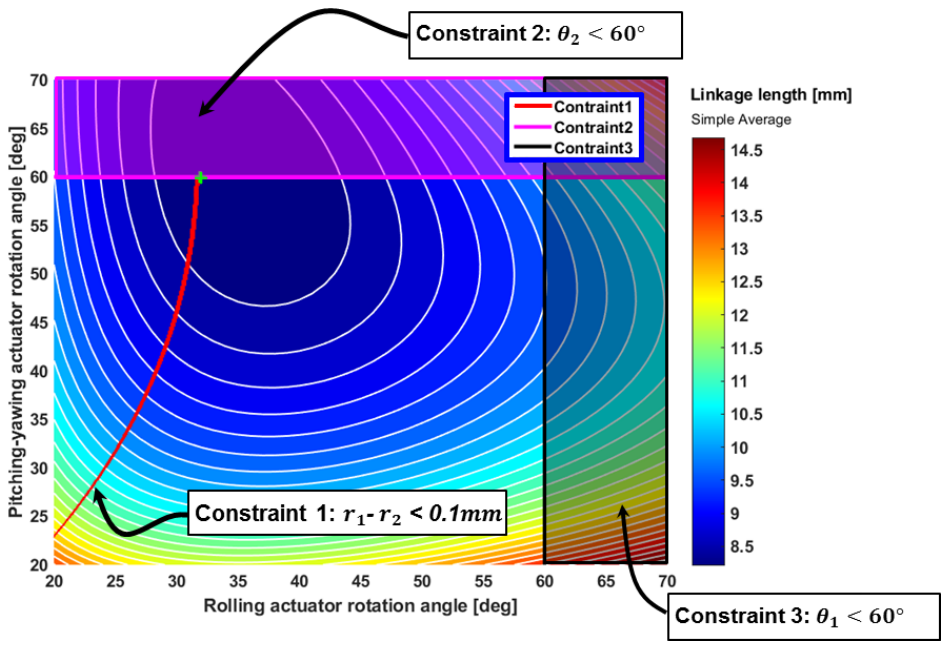

Fig. 2.8 Contour plot: simple average of linkage length

Table 2.1 Specifications of the present TEC

Classification	Value [mm]
Rolling linkage length: r_1	8.2
Pitching-yawing linkage length: r_2	8.3
Length from the upper actuator to main wing axis: h_1	17.6
Length from the lower actuator to main wing axis: h_2	33.3
Multi-DOF link length: h_3	5.4
Intensified free play of the initial configuration	2.6
Intensified free play of the modified configuration	0.9

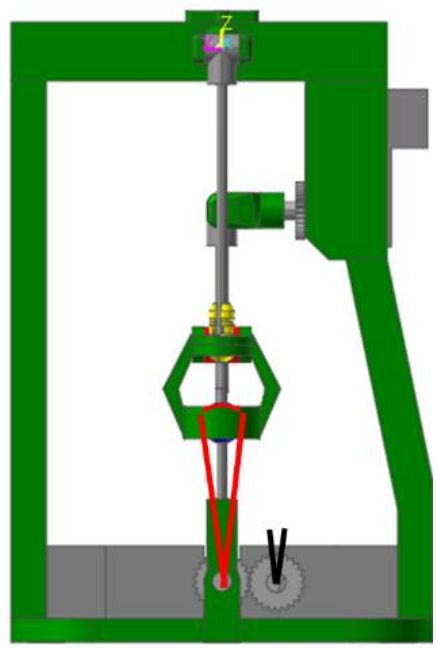

Fig. 2.9 Modified TEC and free play at the present main wing

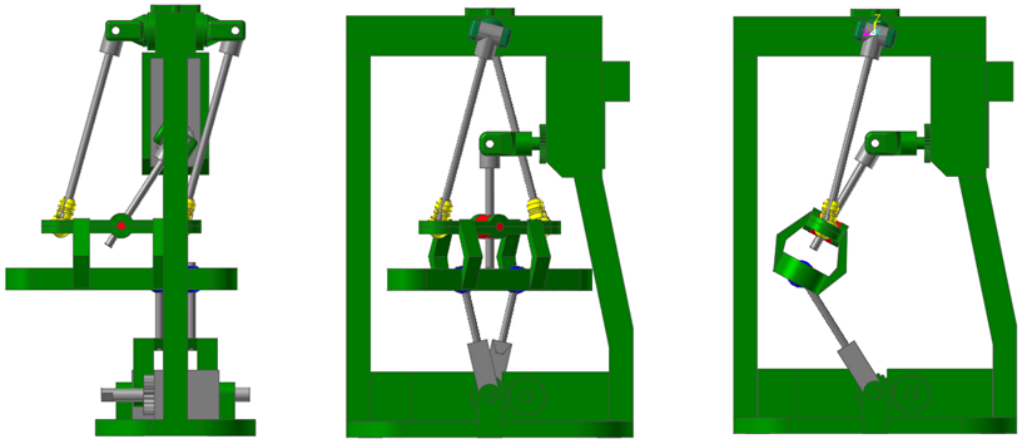

(a) Rolling (b) Yawing (c) Pitching

Figure 2.10 Displacements results by the control input

Chapter 3
Numerical Simulations of FWMAV

3.1 Overview of Numerical Simulation based on Flexible Multibody Dynamics

This section presents the overview of the numerical simulation based on the flexible multibody dynamics. Flexible multibody dynamics analysis is challenging task, due to the geometric nonlinearities of the flexible components combined with the rigid body dynamics, which results in complex problems of nonlinear ordinary differential equations. Thus, iteration techniques are required to solve nonlinearities in the analysis of flexible multibody dynamics.

For the realistic simulation, a number of factors will be considered such as nonlinear elastic effects, multibody characteristics, unsteady aerodynamics and fluid-structural interaction effects [14]. In this thesis, finite element based flexible multi-body analysis tool, DYMORE is adopted [15]. While DYMORE has been usually exploited for the analysis of rotary wing, current research developed a suitable modelling for efficient simulation of insect-type flapping wing via DYMORE. The main wings are modeled by displacement-based geometrically exact one-dimensional beam formulation. Furthermore, two-dimensional cross-sectional analysis is conducted for properties of the beam elements. The present results are validated against the fluid-structural interaction analysis (FSI) considering two-way interactions with flexible structures. Thereafter, numerical simulation of control mechanism is conducted for FWMAV by control inputs: rolling, pitching, and yawing.

3.2 Simulation Setup

The insect-type flapping wing modeling can be simplified to fundamental components that produce aerodynamic forces and following body motions. In this thesis, two main wings,

four joints and two torsional springs are considered for multibody dynamics model as shown in Figure 3.1. For the realistic modelling, torsional spring elements are employed at pitching joints to replicate the free play of the actuator, which may cause instability, degrade controllability of the machinery [10,11] and, by extension, oscillation of each wing that generates undesirable asymmetric aerodynamic forces. The specifications of the actuator are shown as Table 3.1. Torsional spring moment is shown in Figure 3.2. The torsional spring moment is set to zero for the free play region. Thereafter, the moment increases rapidly as the actuator generates torque to resist rotating from the neutral position. Also, the prescribed sinusoidal flapping motion is applied to the main wing, and a passive pitching moment is generated in results.

The flapping mechanism is required to simulate the complete hardware of insect-type flapping wing. Unlike the control mechanism, the flapping mechanism solely generates the flapping motion. A great diversity of the flapping mechanisms was studied by the previous researchers [6,7,16,17]. Among those flapping mechanisms, string based flapping mechanism is employed in this thesis as shown in Figure 3.3. Total weight and flapping amplitude of the flapping mechanism are measured to be 8.2g and 164°, respectively. Also, distance between the main shafts is 15mm. The specifications of the flapping mechanism of the current thesis are shown as Table 3.2.

Table 3.1 Specifications of the Actuator

Classification	Value
Type	Digital
Voltage	3.7 [V]
Torque	0.15 [Nmm]
Speed	0.06 [rad/s]
Turning radius	±60 [°]
Weight with lead and plug	2.18 [g]

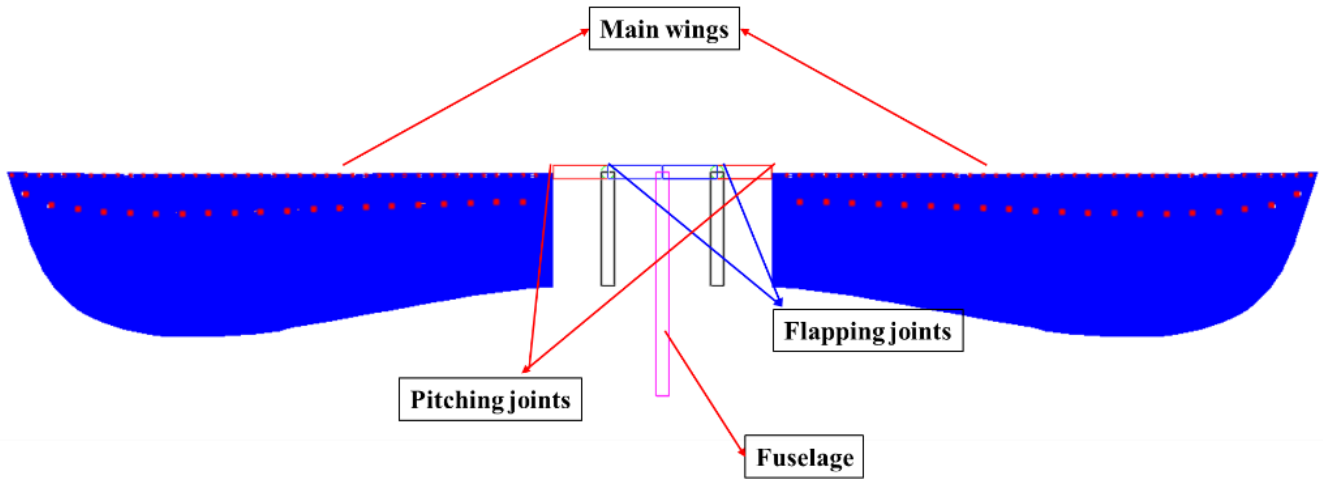

Figure 3.1 Sketch of the present FWMAV

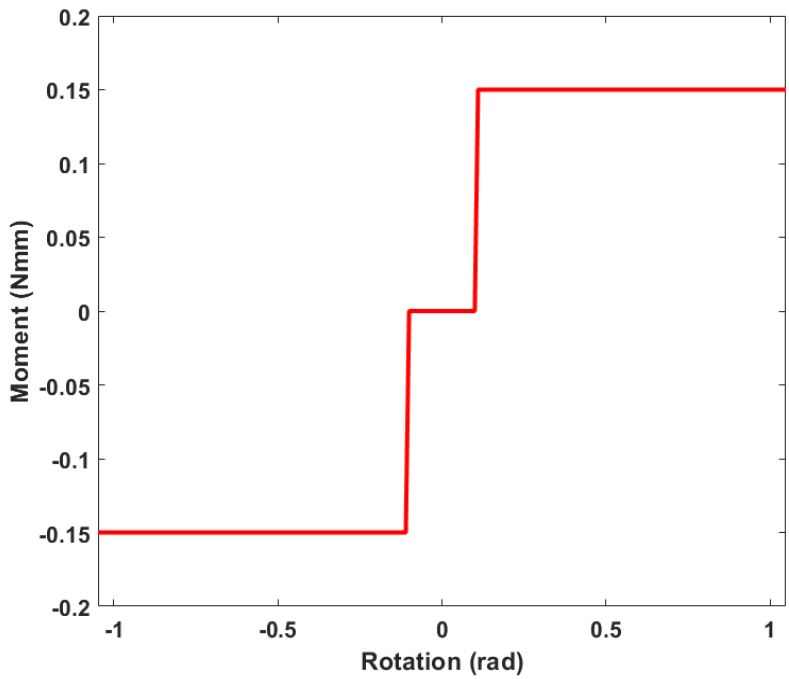

Fig. 3.2 Spring moment in terms of rotation

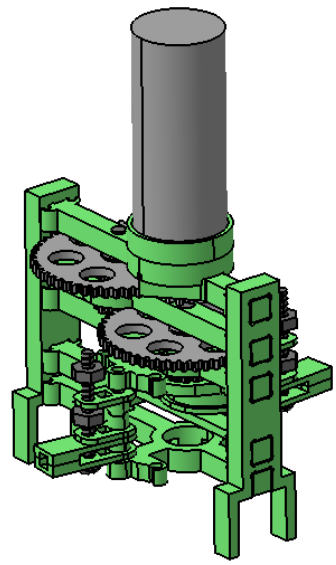

Fig. 3.3 Flapping mechanism [7]

Table 3.2 Specifications of the flapping mechanism

Classification	Value
Power transmission type	String type
Gear material	Plastic
Frame material	Fiber glass sheet
Total weight	8.2 [g]
Flapping amplitude	164 [°]

3.2.1 Simulation Methodology

In order to consider the flexibility of the wing, displacement-based geometrically exact one-dimensional beam model is adopted [18]. Berdichevsky [19] proposed the decomposition of the beam into a linear one-dimensional nonlinear problem and two-dimensional analysis over the cross-section. Thereafter, Bauchau and Han [20] used Hamilton's canonical equation to formulate the beam problems.

Also, the commercially available software, VABS is adopted to analyze cross-section of the main wings. VABS is the VAM (Variational Asymptotic Method) based cross-sectional analysis for composite beam developed by Cesnik and Hodges [21]. Thereafter, Yu and Hodges [22] improved the code for composite beams with arbitrary sections. They employed Timoshenko beam theory for VABS, and demonstrated numerous examples. VABS provides one-dimensional generalized strain, and minimizes two-dimensional strain energy by the obtained generalized strain to deduce the warping function. Throughout such procedures, Timoshenko stiffness matrices will be calculated [23]. Finally, the one-dimensional beam problem is solved by the two-dimensional cross section properties of Timoshenko stiffness matrix obtained.

The design of the main wing has been optimized by experimental study [13]. Also, the configuration of the main wing is depicted in Figure 2.2, and specifications are explained in Table 3.3. The main wings are discretized into 46 components for the cross-sectional analysis as shown in Figure 3.1.

Table 3.3 Specifications of the main wing

Classification	Value
Wing span	70 [mm]
Root chord length	32 [mm]
Camber angle	20 [°]
Carbon rod diameter	1 [mm]
Thickness of the vein	0.5 [mm]

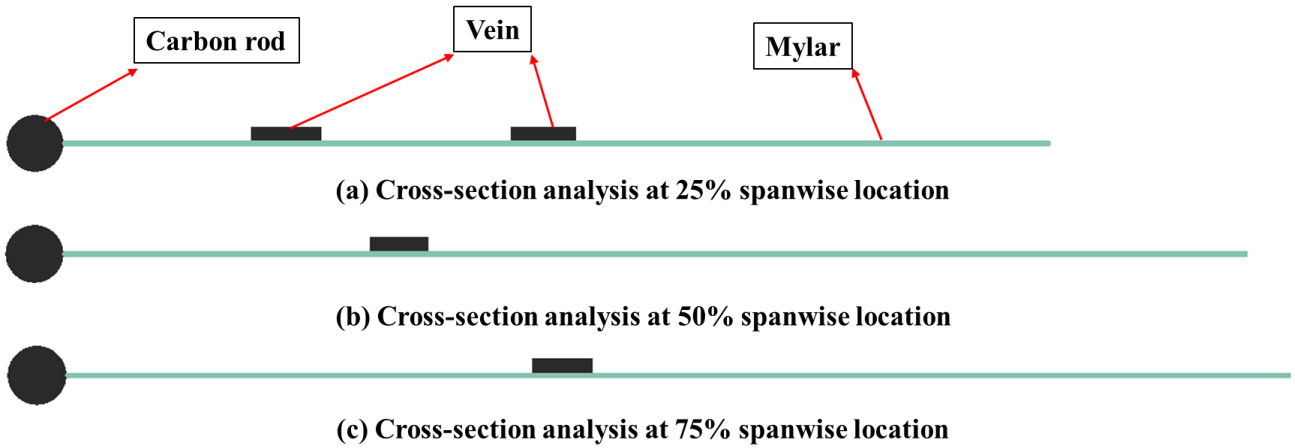

Figure 3.4 Cross-section analysis using VABS

3.2.2 Aerodynamics

In this subsection the present aerodynamic model will be discussed. Gaunaa [24] presented the analytical expression of two-dimensional unsteady thin airfoil theory under the assumptions of incompressible, irrotational, and inviscid flow with regard to rigid body. Thereafter, Peters et al. [25] extended the theory to consider deformable airfoil. For the numerical simulation, Peters' two-dimensional unsteady aerodynamics model is used to calculated the aerodynamic forces and moments with regard to flapping motion. The current method solves the linear potential equation for an arbitrary wing motion. Also, aerodynamic coefficients, lift and drag, are calculated by the modified model of Wang et al [26], which was originally from Dickinson's model [27]. In accordance with Dickinson's empirical model, the lift and drag coefficients can be expressed as shown in Equations (12) and (13). Those coefficients are a function of angle of attack derived by empirical experiences.

$$C_l = 0.225 + 1.58\sin(2.13\alpha - 7.20) \tag{12}$$

$$C_d = 1.92 - 1.55\cos(2.13\alpha - 9.82) \tag{13}$$

Thereafter, Wang et al. [26] modified Dickinson's formulation by comparing experimental and computation results, as shown in Equations (14) and (15). Also, Wang validated such modified aerodynamic function by the three-dimensional experiments.

$$C_l = A\sin(2\alpha) \tag{14}$$

$$C_d = B - C\cos(2\alpha) \tag{15}$$

The coefficients *A, B,* and *C* in the current thesis are derived from aforementioned numerical analysis by DYMORE. Also, the lift and drag coefficient of present thesis is shown in Figures 3.2 and 3.3.

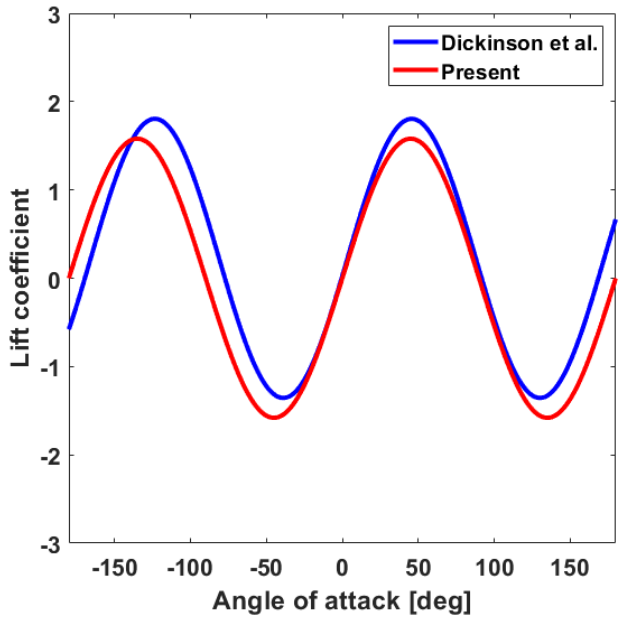

Figure 3.5 Lift coefficient in terms of time

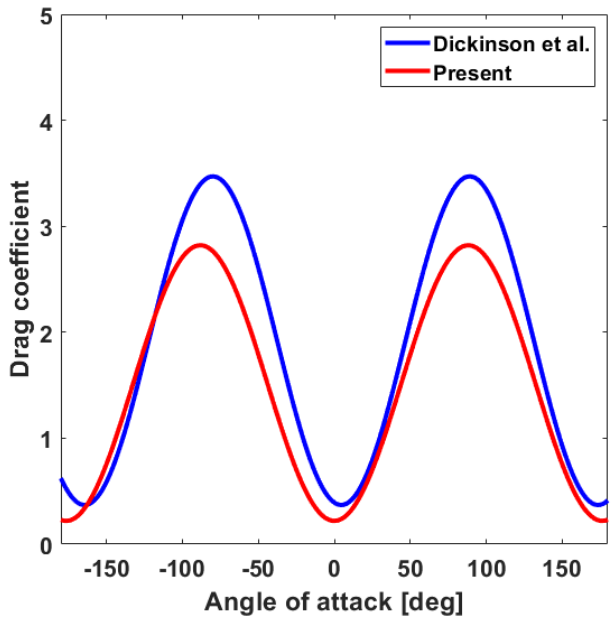

Figure 3.6 Drag coefficient in terms of time

3.3 Numerical simulation

In order to analyze the high frequency flapping wing, studies regarding high fidelity numerical simulation was conducted by previous researchers. Cho et al. [28-29] established computational framework regarding the three-dimensional fluid-structure interaction (FSI) of the flapping wing. They coupled a preconditioned Navier-Stokes solution and a co-rotational (CR) beam analysis to simulate a flapping wing. Thereafter, Yoon et al. [30] studied characteristics of the camber effects of the flapping wing of the aforementioned design. They employed unsteady three-dimensional Navier-Stokes equations for flow solver, and adopted nonlinear finite elements method based on CR formulation for structural solver. The results were compared with previous studies and experimental results for cross-validation.

Present numerical simulation is validated by results of Yoon et al. [30]. The center of gravity of present model is fixed to impose same boundary condition with previous FSI. The simulation operates at sinusoidal flapping angle in frequency of 24Hz and the amplitude of 82°. The averaged thrust is calculated as 6.0gf, which is reasonable compared to the thrust of 6.4gf obtained by previous FSI, as shown in Figures 3.7 and 3.8.

Further verification is performed by thrust measurement at the ground test setup. The overall configuration of the test bed is depicted in Figure 3.9. The span and camber angle of main wing are 125mm and 20°, respectively. Load cell of Table 3.4 is employed for the thrust measurement. The support fixture of Epoxy fiberglass is machined to connect the FWMAV and load cell. For the repeatability of experiments, external power source motives the main motor instead of onboard battery. And the high-speed camera records the overall motion of wing including flapping frequencies as shown in Figure 3.10. Under the input of 2.4V, the FWMAV operates in the flapping frequency of 11.4Hz. Numerical simulation

setup is almost same as previous sections, except that the main wing is discretized into 125 cross sections. The thrust comparison between simulation and experiment shows moderate agreement as depicted in Figure 3.11. The averaged thrust is measured and calculated as 18.84gf and 17.54gf.

Thereafter, control inputs are additionally considered for the numerical simulations to verify feasibility of the present control mechanism. The control moments are estimated at the sinusoidal flapping of 11.4Hz of which amplitude angle is 82°. The main shafts are rotated in accordance with the control inputs as shown in Figure 3.12. The control shaft is visualized as square bar of black line in the figure. Rotational speed of the control shaft is 0.06rad/s as aforementioned descriptions in Table 3.1. The reasonable values of the control moments to maneuver the FWMAV are obtained by control inputs of 9° as explained in Table 3.5. Therefore, the present control mechanism is evaluated to be appropriately designed.

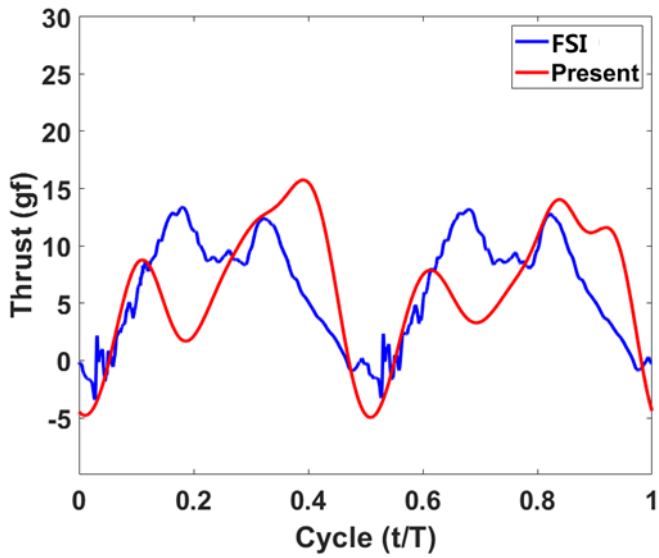

Figure 3.7 Thrust history in terms of time for numerical simulation and FSI

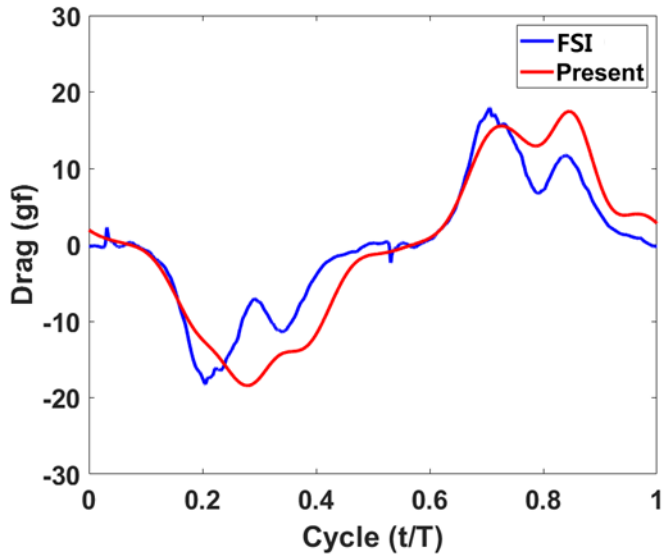

Figure 3.8 Drag history in terms of time for numerical simulation and FSI

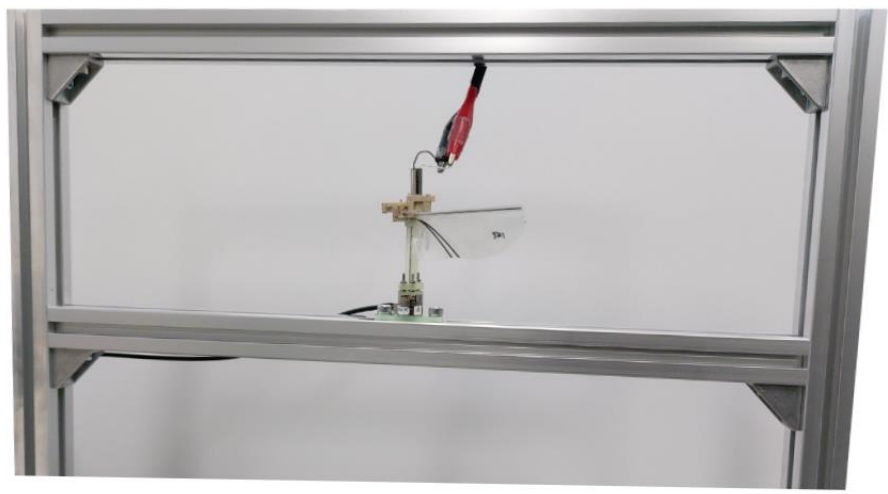

Figure 3.9 Overall configuration of the test bed

Table 3.4 Specifications of the load cell

Force	Sensing ranges	Resolution
F_x	12 [N]	1/320 [N]
F_y	12 [N]	1/320 [N]
F_z	17 [N]	1/320 [N]
T_x	120 [N· mm]	1/64 [N· mm]
T_y	120 [N· mm]	1/64 [N· mm]
T_z	120 [N· mm]	1/64 [N· mm]
Classification	**Values**	
Resonant frequency	7200 [Hz]	

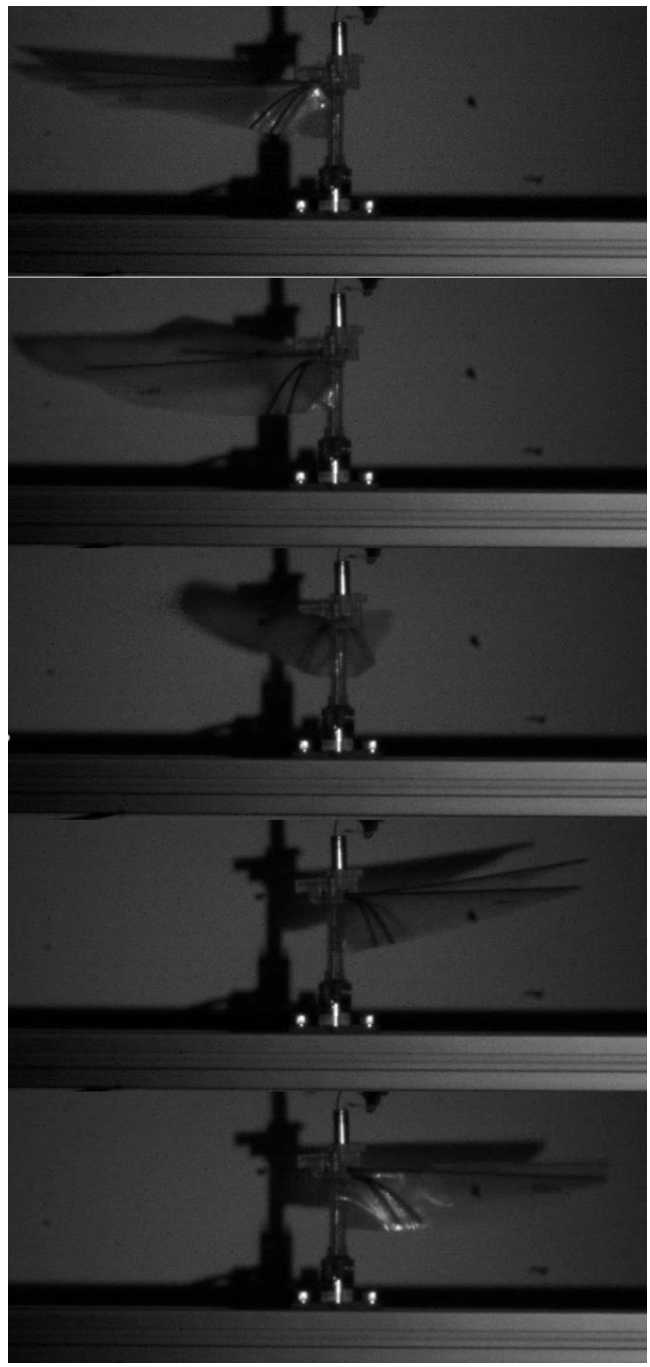

Figure 3.10 High-speed camera recording of the FWMAV

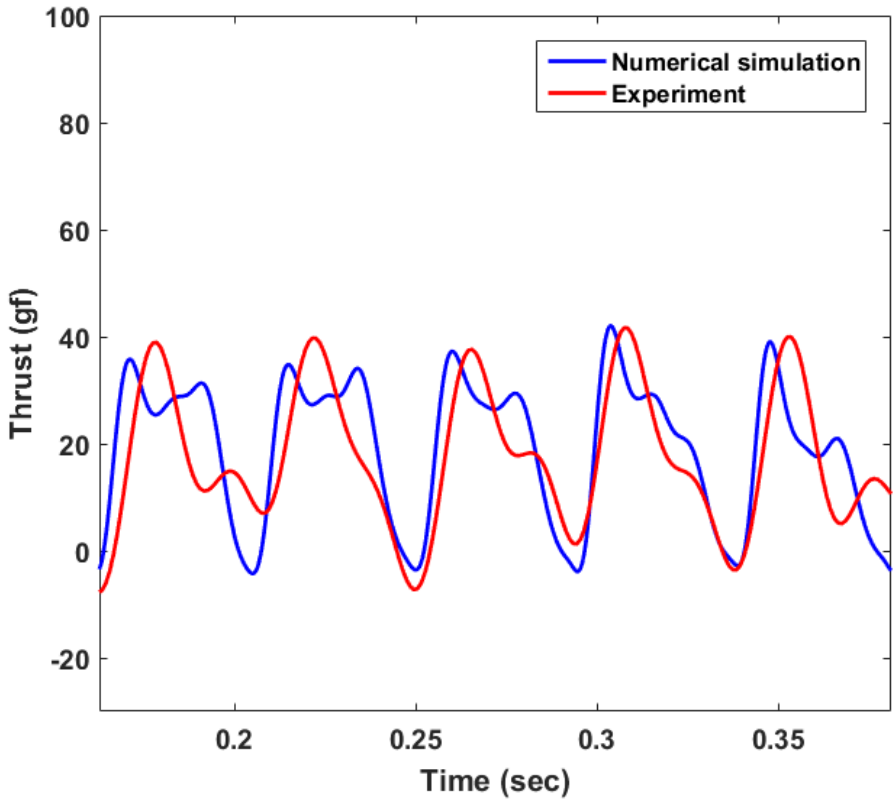

Figure 3.11 Thrust history in terms of time for numerical simulation and experiment

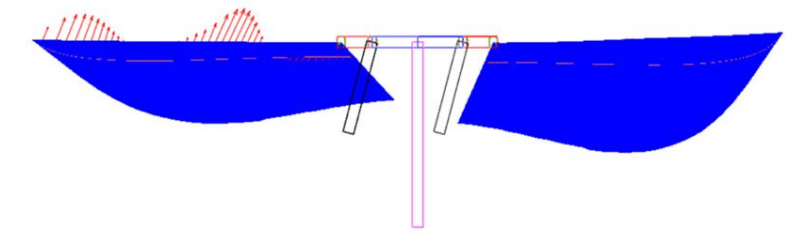

(a) Rolling motion by DYMORE

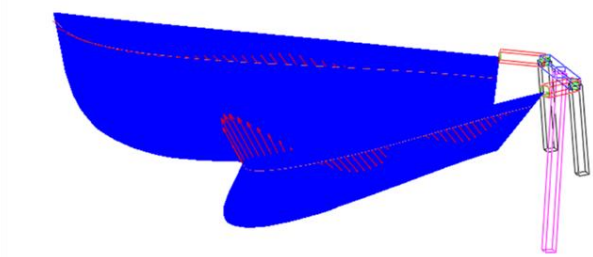

(b) Pitching motion by DYMORE

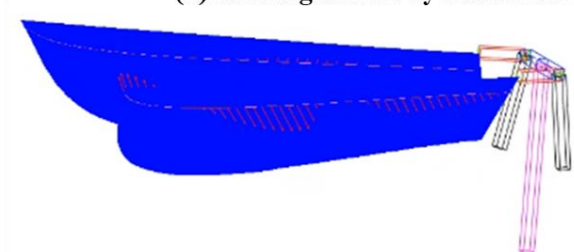

(c) Yawing motion by DYMORE

Figure 3.12 Flapping behavior by the control inputs

Table 3.5 Numerical simulation results

Control input	Twist angle [°]	Numerical simulation results[N· mm]
Rolling	9	1.5
Yawing	9	2.2
Pitching	9	3.6

Chapter 4
Conclusions

4.1 Contributions

Through the thesis, design and simulation of the control mechanism for a tailless FWMAV is performed with the consideration of the free play in main wings. The minimization of free play is achieved by the geometry analysis, and prevention of the undesirable interference between each component is verified by the kinematic simulations. Finally, an adjusted control mechanism is validated by the numerical simulation. The conclusions are obtained as follows:

- Free play is considered through a complete procedure, which occurs in actuators by backlash of the gearbox, causing undesirable aerodynamic forces and resulting instability and degradation of controllability.
- The geometry analysis is conducted to derived specific values of the modified control mechanism, while considering minimization of the free play. The intensified free play of the modified design is decreased to 0.9mm.
- The kinematic simulation is performed to detect interference between each component of the control mechanism. For all the inputs, no interference is detected between each of the three-dimensional components.
- The derived model is numerically simulated to determine effectiveness of modified control mechanisms. Combined with the cross-sectional analysis, geometrically exact beam model is employed for effective simulations. To mimic the free play appropriately, the spring elements are attached to the joints. Gathered control moments are precited as 1.5, 2.2 and 2.6 $\mathrm{N \cdot mm}$ for the rolling, yawing and pitching, respectively, which guarantee proper maneuverability.

4.2 Future Works

There are a few recommended futures works for improvement of the current thesis as follows:

- Kinematic simulation based on the flexible multibody dynamics will be conducted for more realistic behaviors of the control motions.
- The performance of the modified control mechanism will be examined by comparisons with flapping wings by the other researchers from the standpoint of maneuverability.
- Based on the results by the numerical simulation, PID controller will be developed for the stable flight of the current hardware.

Acknowledgments

This research was supported by a grant to Bio-Mimetic Robot Research Center Funded by Defense Acquisition Program Administration, and by Agency for Defense Development

References

[1] Platzer, M. F., and Jones, K. D., “Flapping Wing Aerodynamics: Progress and Challenges,” *AIAA Journal*, Vol. 46, No. 9, 2008, pp. 2136-2149.
doi: 10.2514/1.29263

[2] Yang, W., Wang, L., and Song, B., “Dove: A biomimetic flapping-wing micro air vehicle,” *International Journal of Micro Air vehicles*, Vol. 10, No. 1, 2017, pp. 70-84
doi: 10.1177/1756829317734837

[3] Wood, R. J., "The First Takeoff of a Biologically Inspired At-Scale Robotic Insect," *IEEE Transactions on Robotics,* vol. 24, No. 2, 2008, pp. 341-347.
doi: 10.1109/TRO.2008.916997

[4] Ma, K. Y., Chirarattananon, P., Fuller, S. B., and Wood, R. J., “Controlled flight of a biologically inspired insect-scale robot,” *Science*, Vol. 340, 2013, pp. 603-607.
doi: 10.1126/science.1231806

[5] Keennon, M., Klingebiel, K., Won, H., and Alexander, A., “Development of the Nano Hummingbird: a Tailless Flapping Wing Micro Air Vehicle,” *50th AIAA aerospace sciences meeting including the new horizons forum and aerospace exposition*, 2012, pp. 1-17.
doi: 10.2514/6.2012-588

[6] Phan, H.V., Kang. T., and Park. H.C., “Design and stable flight of a 21g insect-like tailless flapping wing micro air vehicle with angular rates feedback control,” *Bioinspiration & Biomimetics*, Vol. 12, No.3, 2017, pp. 1–17.

doi: 10.1088/1748-3190/aa65db

[7] Gong, D.H., Lee, D.W., Shin, S.J., and Kim, S.Y., "String-based flapping mechanism and modularized trailing edge control system for insect-type FWMAV," *International Journal of Micro Air Vehicles*, Vol. 11, No. 4, 2019, pp. 1-14.
doi: 10.1177/1756829319842547

[8] Hassan, A. M., and Taha, H. E., "Differential-Geometric-Control Formulation of Flapping Flight Multi-body Dynamics," *Journal of Nonlinear Science*, Vol.29, 2019, pp. 1379-1417.
doi: 10.1007/s00332-018-9520-8

[9] Fei, F., Tu, Z., Yang, Y., Zhang, J., and Deng, X., "Flappy hummingbird: An open source dynamic simulation of flapping wing robots and animals," *2019 IEEE International Conference on Robotics and Automation*, Montreal, Canada, 2019.
doi: *10.1109/ICRA.2019.8794089*

[10] Ol, M., Reeder, M., Fredberg, D., McGowan, G., Gopalarathnam, A., & Edwards, J., "Computation vs. Experiment for High-Frequency Low-Reynolds Number Airfoil Plunge," International Journal of Micro Air Vehicles, Vol. 1, No. 2, pp. 99-119, June 2009.
doi: 10.1260/175682909789498279

[11] Ol, M. V., "Vortical Structures in High Frequency Pitch and Plunge at Low Reynolds Number," AIAA Paper 2007-4233, 2007.
doi:10.2514/6.2007-4233

[12] Karásek,M., "Robotic Hummingbird: Design of a Control Mechanism for a Hovering Flapping Wing Micro Air Vehicle," Ph.D. Thesis, Université Libre de Bruxelles, Active Structures Laboratory, Brussels, 2014.

[13] Adhikari, DR., “An Experimental Optimization of Flapping Wing Geometry in the Hover,” Ph.D. Thesis, Seoul National University, 2018.

[14] Altenbuchner, C., and Hubbard, J. E., Jr., “Modern Flexible Multi-Body Dynamics Modeling Methodology for Flapping Wing Vehicles,” Academic Press, Salt Lake City, Utah, 2017.
doi: 10.1016/C2017-0-00911-4

[15] Bauchau, O. A., “DYMORE Users’ Manual,” School of Aerospace Engineering, Georgia Institute of Technology, Atlanta, GA, 2006

[16] Mateti K, Byrne-Dugan RA, Rahn CD, et al. (2013) Monolithic SUEX flapping wing mechanisms for pico air vehicle applications. Journal of Microelectromechanical Systems
doi: 10.1109/JMEMS.2012.2228845

[17] Bolsman, C., Goosen, J., and van Keulen, F., “Design Overview of a Resonant Wing Actuation Mechanism for Application in Flapping Wing MAVs,” International Journal of Micro Air Vehicles, Vol. 1, No. 4, 2009, pp. 263–272.
doi:10.1260/175682909790291500

[18] Bauchau, O. A., Flexible Multibody Dynamics, Springer, Dordrecht, Heidelberg, London, New York, 2011, pp. 617-628.
doi: 10.1007/978-94-007-0335-3

[19] Berdichevsky, V. L., “On the Energy of an Elastic Rod,” *Journal of Applied Mathematics and Mechanics*, Vol. 45, No. 4, 1981, pp. 518–529.
doi: 10.1016/0021-8928(81)90097-6

[20] Bauchau, O. A., and Han, S., “Three-Dimensional Beam Theory for Flexible Multibody Dynamics,” *Journal of Computational and*

Nonlinear Dynamics, Vol. 9, No. 4, Oct. 2014, Paper 041011.
doi:10.1115/1.4025820

[21] Cesnik, C. E. S., and Hodges, D. H., "VABS: A New Concept for Composite Rotor Blade Cross-Sectional Modeling," Journal of the American Helicopter Society, Vol. 42, 1997, pp. 27-38.
doi: 10.4050/JAHS.42.27

[22] Yu, W. and Hodges, D. H., "Generalized Timoshenko Theory of the Variational Asymptotic Beam Sectional Analysis," Journal of the American Helicopter Society, Vol. 50, No. 1, January, 2005, pp. 46-55.
doi: 10.4050/1.3092842

[23] Yu, W., Liao, Lin., Hodges, D. H., and Volovoi, V., "Theory of initially twisted, composite, thin-walled beams," Thin-Walled Structures, Vol 43, No. 8, pp. 1296-1311.
doi: 10.1016/j.tws.2005.02.001

[24] Gaunaa, M., "Unsteady 2D Potential-Flow Forces on a Thin Variable Geometry Airfoil Undergoing Arbitrary Motion," Risø DTU National Lab. for Sustainable Energy, Rept. R-1478, Roskilde, Denmark, July 2006.

[25] Peters, D. A., Hsieh, M. A., and Torrero. A., "A state-space airloads theory for flexible airfoils," Journal of the American Helicopter Society, Vol. 52, No. 4, 2007, pp. 329–342.
doi: 10.4050/JAHS.52.329

[26] Wang, Z. J., Birch, J. M., and Dickinson, M. H., "Unsteady Forces and Flows in Low Reynolds Number Hovering Flight: Two-Dimensional Computations vs

Robotic Wing Experiments," The Journal of Experimental Biology, Vol. 207, No. 3, Jan. 2004, pp. 449–460.
doi: 10.1242/jeb.00739

[27] Dickinson, M. H., Lehmann, F. O., and Sane, S. P., "Wing Rotation and the Aerodynamic Basis of Insect Flight," Science, Vol. 284, No. 5422, 1999, pp. 1954–1960.
doi: 10.1126/science.284.5422.1954

[28] Cho, H., Lee, N., Kwak, J. Y., Shin, S. J., and Lee, S., "Three-dimensional Fluid-Structure Interaction Analysis of a Flexible Wing under the Simultaneous Pitching and Plunging Motion," Nonlinear Dynamics, Vol. 86, No.3, 2016, pp. 1951-1966.
doi: 10.1007/s11071-016-3007-7

[29] Cho, H., Lee, N., Shin, S. J., Lee, S., and Kim, S., "Improved Computational Approach for 3-D Realistic Insect-like Flapping Wing using Co-rotational Finite Elements," 55th AIAA Aerospace Sciences Meeting, 2017, p. 1417.
doi: 10.2514/6.2017-1417

[30] Yoon, S. H., Cho, H., Lee, J., Kim, C., and Shin, S. J., "Effects of camber angle on aerodynamic performance of flapping-wing micro air vehicle," Journal of Fluids and Structures, Vol. 97, 2020.
doi: 10.1016/j.jfluidstructs.2020.103101

국문초록

유격을 고려한 무미익 초소형 날갯짓 비행체 통합 설계: 기하분석 및 수치 해석을 통한 접근

최재원

서울대학교 대학원

우주시스템 협동과정

곤충 모방형 날갯짓 비행체는 꼬리날개가 없기 때문에 새 모방형 날갯짓 비행체와 비교하여 가볍고 작게 설계될 수 있다. 그러나, 곤충 모방형 날갯짓 비행체는 꼬리날개가 없다는 특징으로 인하여, 오직 두 날개만을 이용하여 조종력을 발생시킨다. 따라서, 이에 대한 많은 연구가 수행되었고 개발된 여러 자세 제어 방법 중 본 학위 논문에선 날개 끝단 비틀림을 이용한 자세 제어 장치를 다룬다. 해당 방법은 주날개의 뿌리 부분을 자세 제어 장치와 연결하고 이를 회전시켜 날개 끝단에 변형을 발생시킨다. 자세 제어 장치에는 경량화를 위하여 가볍고 작은 장비들이 사용된다. 그러나, 자세 제어 장치 제작에 사용되는 초소형 구동기는 작은 크기로 인하여 내부 기어에 백래시를 갖고 있다. 따라서, 이는 주날개의 불필요한 유격을 발생시킬 수 있다.

이러한 유격은 주날개의 진동으로 이어져, 불필요한 비대칭적 공력을 발생시킬 수 있다.

이러한 상황 때문에 유격이 최소화된 자세 제어 장치 설계를 수행하였다. 첫째로, 기하학적 해석을 통하여 유격에 영향을 주는 요인을 파악하였다. 이를 통하여 유격을 최소화한 설계를 도출하였으며, 3 차원 computer aided design (CAD) 형상과 RecurDyn 을 이용하여 동역학적 해석을 수행하였다. 이를 통하여 자세 제어 장치의 구동 중 발생하는 간섭을 확인하였다. 최종적으로, 수치적 시뮬레이션을 이용하여 개선된 자세 제어 장치의 타당성을 확인하였다. 이때, 주날개는 변위 기반 기하학적 정밀 보로 모델링 되었으며, 2 차원 단면 해석 결과를 사용하여 해석을 수행하였고 공력 모델은 2 차원 비정상 모델을 사용하였다. 또한, 유격을 모사하기 위하여 스프링 요소를 관절에 삽입하여 해석을 수행하였다. 결과적으로, 본 연구에서 설계한 자세 제어 장치가 유효한 조종력을 발생시키는 것을 확인하였다.

주요어 : 곤충 모방형 날갯짓 비행체, 유격, 기하학적 해석, 동역학적 시뮬레이션, 최소화, 수치적 시뮬레이션

학 번 : 2019-22226